Volume 49
Number 37
7 October 2020
Pages 12881-13186

Dalton Transactions

An international journal of inorganic chemistry

rsc.li/dalton

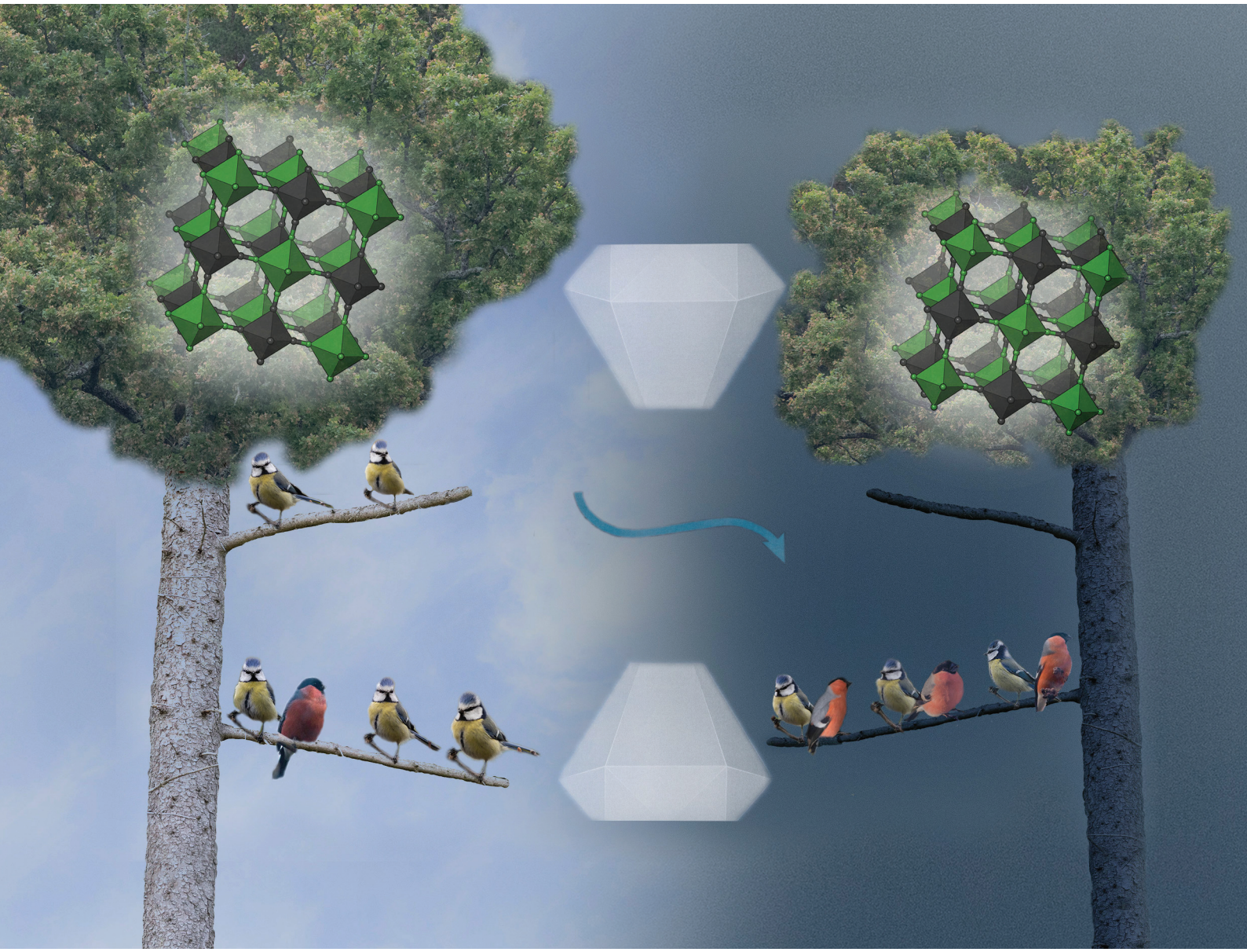

ISSN 1477-9226

ROYAL SOCIETY OF CHEMISTRY

COMMUNICATION

Hanna L. B. Boström, Ines E. Collings *et al.*

Spin crossover in the Prussian blue analogue $FePt(CN)_6$ induced by pressure or X-ray irradiation

Dalton Transactions

ROYAL SOCIETY OF CHEMISTRY

COMMUNICATION

View Article Online
View Journal | View Issue

Cite this: *Dalton Trans.*, 2020, **49**, 12940

Received 7th June 2020,
Accepted 9th July 2020

DOI: 10.1039/d0dt02036b

rsc.li/dalton

Spin crossover in the Prussian blue analogue $FePt(CN)_6$ induced by pressure or X-ray irradiation†

Hanna L. B. Boström, *[a] Andrew B. Cairns, [b] Lei Liu, [c] Peter Lazor[c] and Ines E. Collings *[d]

The spin state of the Prussian blue analogue $Fe^{II}Pt^{IV}(CN)_6$ is investigated in response to temperature, pressure, and X-ray irradiation. While cooling to 10 K maintains the high-spin state of Fe^{II}, compression at ambient temperature induces a first-order spin-crossover (SCO) transition with a small hysteresis loop ($p\uparrow$ = 0.8 GPa, $p\downarrow$ = 0.6 GPa). In addition, the high-spin to low-spin transition can be initiated at lower pressure through increased X-ray irradiation. Our study highlights a cooperative SCO with moderate pressure in a porous Prussian blue analogue.

Material bistability is exploited in a range of applications, since it gives access to two distinct physical property states, which can be reversibly switched by external stimuli, *e.g.* temperature, pressure, or light irradiation.[1] In this regard, spin crossover (SCO) materials are of interest since their transitions between high-spin (HS) and low-spin (LS) states are coupled with changes in their magnetic, optical, and structural properties.[2–4] In addition, the HS/LS bistability in porous SCO materials can be further controlled by the insertion/removal of different guest molecules.[5,6] The SCO phenomenon is most commonly observed for octahedral Fe^{II} ions that coordinate to nitrogen-containing ligands, forming molecular species or polymeric structures.[7] If the interaction between spin crossover centres is sufficiently strong—*i.e.* the cooperativity is high—the SCO transition tends to be abrupt and can additionally exhibit hysteresis.[7,8] Such transitions are ideal for switching devices, particularly if the bistable regime occurs at room temperature.[9]

A useful strategy to increase the abruptness of SCO transitions is to incorporate the SCO-active metal centres in a coordination polymer, as the electron–phonon coupling enhances the cooperativity.[7,10] A family of coordination polymers suitable for cooperative SCO transitions are the Prussian blue analogues (PBAs).[11] Reminiscent of double perovskites, they exhibit the formula $A_xM[M'(CN)_6]_y$, where A is an alkali metal and M/M′ are transition metals. Due to their stoichiometric and compositional flexibility, PBAs are associated with a range of intriguing magnetic and electronic functionality.[12,13] In particular, metal–metal charge transfer, which can also be accompanied by a spin transition, under various stimuli has been intensely studied in $A_xM[Fe(CN)_6]_y$ (M^{II} = Mn or Co),[14–18] as well as related molecular complexes.[12,19,20] As the rigidity and porosity of PBAs can be tuned by varying the stoichiometry, these systems constitute an interesting field for the exploration of cooperative SCO behaviour.

However, PBAs that exhibit spin crossover without metal charge transfer are rare and, to the best of our knowledge, only two examples are currently known. First, $CsFeCr(CN)_6$ undergoes a SCO transition induced by temperature, pressure, or X-ray irradiation,[21–23] and several theoretical studies have been devoted to this compound.[24,25] We note that the related compounds, $Fe_3[Cr(CN)_6]_2$ and $K_{0.4}Fe_4[Cr(CN)_6]_{2.8}\cdot 16H_2O$, also exhibit SCO, although these are initiated by linkage isomerism of the CN^- where the Fe–NC bonding changes to Fe–CN.[26,27] Second, Halder *et al.* reported pressure-induced SCO in $FePt(CN)_6$ as part of a conference abstract, but this was not explored in detail.[28] $FePt(CN)_6$ crystallises in the high-symmetry space group $Fm\bar{3}m$ and does not feature A-site cations or vacancies.[29] Consequently, it lacks the disorder that often complicates the study of other PBAs—including $CsFeCr(CN)_6$.[24,30] In addition, Pt^{IV} is not susceptible to the electron transfer that

[a]*Department of Chemistry—Ångström Laboratory, Uppsala University, Box 538, 751 21 Uppsala, Sweden. E-mail: hanna.bostrom@kemi.uu.se*
[b]*Department of Materials, Imperial College London, Royal School of Mines, Exhibition Road, SW7 2AZ, UK*
[c]*Department of Earth Sciences, Uppsala Universitet, Villavägen 16, 752 36 Uppsala, Sweden*
[d]*Centre of X-ray Analytics, Empa – Swiss Federal Laboratories for Materials Science and Technology, Überlandstraße 129, 8600 Dübendorf, Switzerland. E-mail: ines.collings@empa.ch*

†Electronic supplementary information (ESI) available: Experimental details, Curie–Weiss plot, diffraction patterns and cell parameters under variable pressure and X-ray exposure, Fe–N bond lengths as a function of pressure, Birch–Murnaghan EoS fits, *f–F* plots and Raman spectra under variable pressure. The low-spin structure of $FePt(CN)_6$ has been deposited to the ICSD with the number 2006568. See DOI: 10.1039/D0DT02036B

may take place if M′ = Fe^{III}.[14–16,31] As a result, $FePt(CN)_6$ is a useful model system for further exploration of SCO transitions in PBAs. Here, we expand on the results presented in ref. 28 and present a study of the spin state of $FePt(CN)_6$ in response to temperature, pressure, and X-ray irradiation. We show that the SCO transition in $FePt(CN)_6$ may be induced by compression to 0.8(1) GPa or at lower pressures upon continued X-ray irradiation, but not thermally. The results are contrasted with the behaviour of $CsFeCr(CN)_6$.

The magnetic properties of $FePt(CN)_6$ were investigated in the range 300–10 K with a magnetic field strength, H, of 5000 Oe and a cooling rate of 2 K min^{-1}. Curie–Weiss analysis [Fig. S1†] gives an effective magnetic moment of 5.50 μ_B, in line with the value expected for high spin Fe^{II} with incomplete quenching of the orbital angular momentum.[32] The temperature dependence of the magnetic moment follows the behaviour expected for a paramagnet, with no indication of magnetic order or spin crossover [Fig. 1]. Previous studies indicate that spin crossover transitions below ~100 K may be very slow due to the insufficient thermal energy relative to the energy difference between the HS and LS states.[3,33–35] Thus, we cannot exclude that $FePt(CN)_6$ remains kinetically trapped in the HS state. The Weiss constant is −0.8(6) K, which agrees with the absence of any magnetic order. Overall, the results indicate that (i) the magnetic interactions between the unpaired spins of Fe^{II}(HS) in $FePt(CN)_6$ are sufficiently weak to give paramagnetic behaviour without magnetic phase transitions, and (ii) there is no thermally induced spin crossover transition. This is in contrast to $CsFeCr(CN)_6$ that exhibits magnetic ordering below 9 K and a spin crossover transition at 211 K upon cooling.[21]

Variable-pressure X-ray diffraction (XRD) was carried out in the range 0–3 GPa using both Daphne oil and methanol as pressure-transmitting media (PTM). These PTMs were chosen to contrast the SCO behaviour when compressed in a non-penetrating (oil) and a penetrating (MeOH) PTM, since the SCO can be influenced by the presence of guest molecules.[5] At ambient pressure, $FePt(CN)_6$ adopts the cubic space group $Fm\bar{3}m$ with a = 10.60767(5) Å. The lattice parameter decreases continuously until 0.83 GPa, where a second cubic phase (a = 10.2008(3) Å) appears, consistent with a SCO transition [Fig. 2(a)]. The coexistence of HS and LS phases only occurred for this pressure point, with the increase of 0.1 GPa leading to the complete conversion to the LS state. At the HS/LS coexistence, the unit cell volume reduces by ~10% due to the spin crossover, resulting from the shortening of the Fe–N bonds by *ca.* 0.2 Å during the transition [Fig. S3†]. This is similar in magnitude to what was reported for other SCO complexes based on nitrogen-coordinated Fe^{II}.[3,36] The critical pressure agrees with the results from ref. 28 at 0.9(1) GPa. The abrupt volume discontinuity on going from HS to LS suggests a first-order spin transition.[8] No further transitions are observed upon compression and the LS cubic phase persists up to 3 GPa. This contrasts with the isostructural $MnPt(CN)_6$, which exhibits a displacive phase transition at 1.31(10) GPa.[37] Upon decompression, the LS state reverts to HS at 0.63(3) GPa, thus the pressure-induced SCO is associated with a small hysteresis of *ca.* 0.2 GPa.

The bulk moduli (B_0), as calculated by second-order Birch–Murnaghan equation-of-state (EoS) fits using EoSFit,[38–40] show a dependence on the pressure-transmitting medium [Fig. 2(a)]. The HS phase exhibits similar bulk moduli for both PTMs at 33(5) GPa and 29(2) GPa for Daphne oil and MeOH, respect-

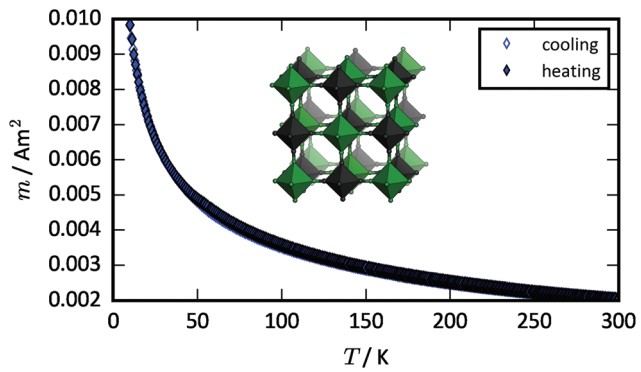

Fig. 1 The temperature dependence of the magnetic moment, m, measured at H = 5000 Oe. Data collected on cooling (heating) are shown in empty (filled) symbols. Inset shows the structure of $FePt(CN)_6$ with green and black octahedra representing FeN_6 and PtC_6, respectively.

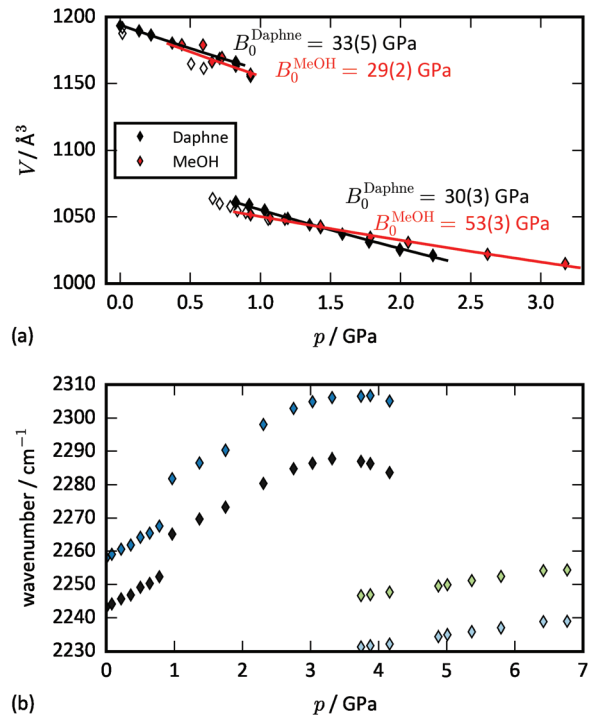

Fig. 2 The pressure dependence of the unit cell volume of $FePt(CN)_6$ with filled (empty) symbols referring to compression (decompression) data. Solid lines represent second-order Birch–Murnaghan equation-of-state fits with the bulk moduli given for compressions in Daphne oil (black) and methanol (red). Error bars are smaller than the marker size. (b) Evolution of the vibrational modes of the cyanide linkers as a function of pressure.

ively. Due to the few data points in the low-pressure regime for the HS phase compressed in MeOH, the V_0 value was fixed to the V_0 refined from the ambient measurement, reducing the error on the bulk modulus. By way of context, these values are similar in magnitude to those of $K_{0.25}Ni[Cr(CN)_6]_{0.75}\cdot 2.35D_2O$ (31 GPa) and $Ni[Fe(CN)_6]_{2/3}$ (25 GPa) nanoparticles,[41,42] yet slightly lower than the values for $MnPt(CN)_6\cdot xH_2O$ (35 GPa) and $CuPt(CN)_6\cdot xH_2O$ (37 GPa).[37] Within the LS state, however, the choice of PTM has a considerable effect on the volume pressure dependence with B_0 = 30(3) GPa or 53(3) GPa when compressed in Daphne oil or MeOH, respectively. This suggests that inclusion of MeOH occurs upon compression, but that only in the LS state does its presence impact on the compressibility. This behaviour is reminiscent of the guest-dependent thermal expansion properties of related PBAs, for which only $ZnPt(CN)_6\cdot 2H_2O$ exhibits guest-dependent thermal expansion while $CdPt(CN)_6\cdot 2H_2O$ that contains larger pore sizes is not affected by the presence of water.[43] Indeed, the solvent-accessible void volume of $FePt(CN)_6$ at 52 Å^3 per cavity (at 0.9 GPa) decreases by 12 Å^3 upon the SCO transition, as calculated in PLATON.[44] The van der Waals volume of MeOH at 36 Å^3 (ref. 45) allows one molecule of MeOH to easily fit within each cavity. However, the superfilling of MeOH is not observed, unlike the pressure behaviour of more flexible metal–organic frameworks that can exhibit an increase in pore volume when compressed in MeOH media.[46,47]

The high-pressure behaviour of $FePt(CN)_6$ was also investigated with Raman spectroscopy using silicone oil as the PTM [Fig. S10 and S11†]. At ambient pressure, the spectra contain two peaks at 2242 and 2258 cm^{-1} [Fig. 2(b)], corresponding to the cyanide-stretching E_g and A_{1g} modes, respectively.[48] Upon compression, these vibrations gradually stiffen and a discontinuous shift to higher wavenumber occurs at 0.9(1) GPa. This transition is consistent with the critical pressure for the SCO transition as found by XRD. The change in vibrational frequency can be explained by considering the nature of the Fe–N bond. As Fe^{II} changes from the HS to the LS spin state, the e_g orbital is depopulated. This enhances the σ-donation from the antibonding σ-orbital located at N, thereby strengthening the CN bond.[49] At 3.3 GPa, additional vibrational modes appear at *ca.* 2250 cm^{-1} which become more pronounced at the next pressure of 3.7 GPa, suggesting a first-order structural phase transition. These spectral features increase in intensity upon further compression to 6.77 GPa, whilst the absorption lines corresponding to the LS state of $FePt(CN)_6$ broaden substantially. Significant hysteresis is observed as pressure is released, with signals from the highest-pressure phase persisting down to 1.33 GPa. However, the system reverts to the cubic LS state at 1 GPa and the HS state is recovered on decompression to 0.08 GPa. Overall, the Raman spectra agree well with the XRD data and suggest high-pressure XRD studies above 3 GPa as an interesting avenue for further exploration.

The spin transition can also be induced by continuous X-ray irradiation under modest compression (0.6 GPa). This serendipitous finding occurred due to the collection of 112 successive frames (4 s exposure each) as a single-crystal collection macro was initiated. Initially, $FePt(CN)_6$ is exclusively in the HS state with a = 10.5489(11) Å. During the first 30 s, the cell dimensions contract to 10.4986(9) Å without significant reflection broadening [Fig. 3(a) and Fig. S9†]. Similar behaviour is observed in the X-ray induced spin transition of $CsFeCr(CN)_6$, where the unit cell contracts prior to the SCO, although it is accompanied by peak broadening.[22] After 30 s of continuous X-ray irradiation, the LS phase emerges in the XRD patterns and its phase fraction rapidly grows upon further irradiation [Fig. 3(b)]. After 2.5 minutes, the LS phase fraction reaches *ca.* 70% and the rate of SCO slows down dramatically. Following the completion of the irradiation (corresponding to 8 min of exposure), the system comprises ~85% LS phase. With the small X-ray beam size used, a different region of the sample was measured next (at the same pressure point) that had not been exposed to X-rays. This diffraction pattern exhibits only the HS state [Fig. S9†], indicating that the spin transition is initiated by the X-rays and not by kinetic factors. The HS/LS fraction evolution with X-ray irradiation shows an anomaly at 200 s, where there is a peak of the HS state, in contrast to its overall decreasing trend. This may be caused by some unirradiated sample entering the beam path, since the diffraction patterns are obtained at different rotation angles of the diamond anvil cell.

It is not clear whether the X-ray induced spin transitions observed in $FePt(CN)_6$—or in $CsFeCr(CN)_6$ [22]—are reversible. Reversible SCO induced by radiation (light, soft and hard X-rays) have been previously observed but at low temperature,

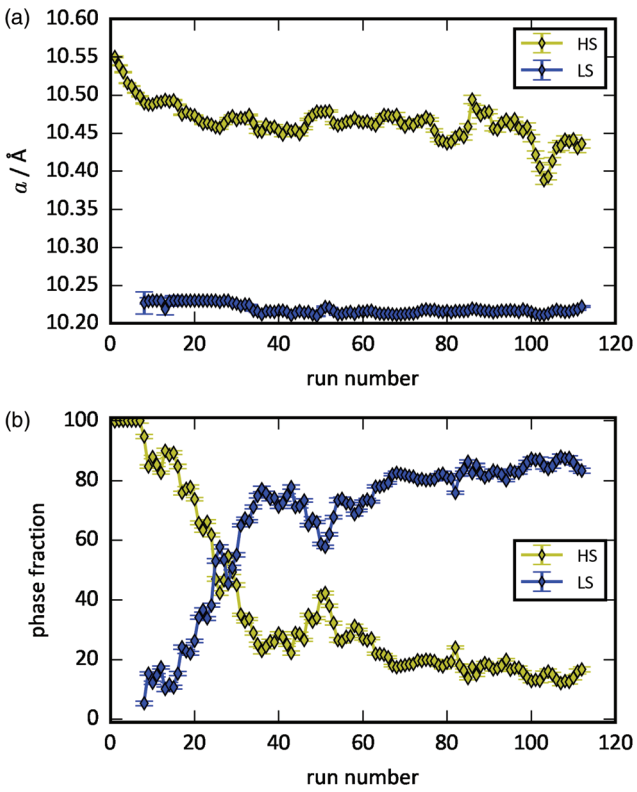

Fig. 3 The (a) lattice parameters and (b) phase fractions of the HS phase (yellow) and LS phase (blue) as a function of X-ray exposure time.

where radiation exposure causes an excitation to the HS state.[50–53] Irreversible spin changes induced by radiation are less documented, but could involve local structural and/or chemical changes in addition to the spin transition.[50,54] In our case, measurements upon decompression would help ascertain the reversibility of the spin change observed from radiation. Given previous experiments that indicate the sensitivity of PBAs to X-ray radiation, *e.g.* prevention of structural phase transitions upon extended X-ray exposures,[37] it is likely that X-ray radiation induces an irreversible spin transition, although further studies are needed.

While the Prussian blue analogues $FePt(CN)_6$ and $CsFeCr(CN)_6$ both exhibit spin crossover behaviour, the energy scales associated with these processes are different. $CsFeCr(CN)_6$ shows a thermally induced transition that may be brought close to room temperature by applying a pressure of ~1 kbar.[22] In contrast, the HS state of $FePt(CN)_6$ is retained down to 10 K—although kinetic trapping is conceivable—and nearly 1 GPa is required to trigger the spin state switching at ambient temperature. The discrepant behaviours indicate different Fe^{II} orbital energies in these two PBAs, which likely arises from electronic—rather than steric—effects, since the ionic radii of Pt^{IV} and Cr^{III} are nearly identical.[55] Another key difference between the two PBAs is the presence of Cs ions in $CsFeCr(CN)_6$, in contrast to the open nature of $FePt(CN)_6$. Extra-framework cations can exert a strong influence on the dynamics of the framework,[56] which may also affect the electronic structure. Thus, local-structure and computational studies would help rationalise the effects of varying chemistry (*e.g.* Cr^{III} *vs.* Pt^{IV}) on the SCO behaviour of iron-containing PBAs.

To conclude, the spin crossover transition in $FePt(CN)_6$ is thermally inaccessible, but may be induced by pressure, with initiation of the spin change possible at lower pressures by X-ray irradiation. Although we note that the reversibility of the latter is not known. Consequently, the spin transition in $FePt(CN)_6$ is associated with a larger energy scale than $CsFeCr(CN)_6$ and so requires harsher conditions to be initiated. It is striking that only two PBAs with SCO transitions and no metal charge transfer have been reported so far, especially considering the interest in switchable electron transfer in these materials.[15] While many PBAs based on $Fe(CN)_6^{3/4-}$ moieties favour inter-metal charge transfer reactions,[14,16,31] this is evidently not the case for $Cr(CN)_6^{3-}$ or $Pt(CN)_6^{2-}$. Likewise, $Co(CN)_6^{3-}$ may also be expected to resist internal redox by virtue of its stable LS d^6 configuration. As the A and M′ cations, stoichiometry, and hydration level are tuneable parameters, there is a large scope for the development of structure–property relationships and functional optimisation of SCO behaviour at ambient conditions. Consequently, further exploration of spin crossover transitions in Prussian blue analogues will be an intriguing avenue of research.

Conflicts of interest

There are no conflicts to declare.

Acknowledgements

Dedicated to the memory of Harold A. Goodwin (UNSW, 1935-2020). We thank DESY and Diamond Light Source for beamtime (EE19776) and Dominik Daisenberger, Anna Pakhomova and Baptiste Journaux for assistance with data collection. IEC thanks the European Union's Horizon 2020 research and innovation programme under the Marie Skłodowska-Curie grant agreement number 754364 for funding. Andrew Goodwin (Oxford) is gratefully acknowledged for the use of lab facilities and Roland Mathieu (Uppsala) for helping with the magnetometry. Ingegerd Boström Carlsson is gratefully acknowledged for creation of the cover image.

References

1 Z.-S. Yao, Z. Tang and J. Tao, *Chem. Commun.*, 2020, **56**, 2071–2086.
2 R. W. Hogue, S. Singh and S. Brooker, *Chem. Soc. Rev.*, 2018, **47**, 7303–7338.
3 J. A. Real, A. B. Gaspar and M. C. Muñoz, *Dalton Trans.*, 2005, 2062–2079.
4 O. Kahn and C. Jay Martinez, *Science*, 1998, **279**, 44–48.
5 P. D. Southon, L. Liu, E. A. Fellows, D. J. Price, G. J. Halder, K. W. Chapman, B. Moubaraki, K. S. Murray, J.-F. Létard and C. J. Kepert, *J. Am. Chem. Soc.*, 2009, **131**, 10998–11009.
6 Z.-P. Ni, J.-L. Liu, M. N. Hogue, W. Liu, J.-Y. Li, Y.-C. Chen and M.-L. Tong, *Coord. Chem. Rev.*, 2017, **335**, 28–43.
7 P. Gütlich, Y. Garcia and H. A. Goodwin, *Chem. Soc. Rev.*, 2000, **29**, 419–427.
8 W. Nicolazzi and A. Bousseksou, *C. R. Chim.*, 2018, **21**, 1060–1074.
9 A. Bousseksou, G. Molnár, P. Demont and J. Menegotto, *J. Mater. Chem.*, 2003, **13**, 2069–2071.
10 M. C. Muñoz and J. A. Real, *Spin-crossover materials: properties and applications*, Wiley, Oxford, 2013, ch. 4, pp. 121–146.
11 H. J. Buser, D. Schwarzenbach, W. Petter and A. Ludi, *Inorg. Chem.*, 1977, **16**, 2704–2710.
12 D. Li, R. Clérac, O. Roubeau, E. Harté, C. Mathonière, R. LeBris and S. M. Holmes, *J. Am. Chem. Soc.*, 2008, **130**, 252–258.
13 H. Tokoro and S.-i. Ohkoshi, *Dalton Trans.*, 2011, **40**, 6825–6833.
14 O. Sato, T. Iyoda, A. Fujishima and K. Hashimoto, *Science*, 1996, **272**, 704–705.
15 D. Aguilà, Y. Prado, E. S. Koumousi, C. Mathonière and R. Clérac, *Chem. Soc. Rev.*, 2016, **45**, 203–224.
16 Y. Moritomo, M. Hanawa, Y. Ohishi, K. Kato, M. Takata, A. Kuriki, E. Nishibori, M. Sakata, S. Ohkoshi, H. Tokoro and K. Hashimoto, *Phys. Rev. B: Condens. Matter Mater. Phys.*, 2003, **68**, 144106.
17 G. G. Levchenko, L. V. Berezhnaya, G. G. Filimonov and W. Han, *J. Phys. Chem. B*, 2018, **122**, 6846–6853.
18 V. Escax, A. Bleuzen, J. P. Itié, P. Munsch, F. Varret and M. Verdaguer, *J. Phys. Chem. B*, 2003, **107**, 4763–4767.

19 N. Daffé, J.-R. Jiménez, M. Studniarek, A. Benchohra, M.-A. Arrio, R. Lescouëzec and J. Dreiser, *J. Phys. Chem. Lett.*, 2019, **10**, 1799–1804.
20 Y. Sekine, M. Nihei, R. Kumai, H. Nakao, Y. Murakami and H. Oshio, *Chem. Commun.*, 2014, **50**, 4050–4052.
21 W. Kosaka, K. Nomura, K. Hashimoto and S. Ohkoshi, *J. Am. Chem. Soc.*, 2005, **127**, 8590–8591.
22 D. Papanikolaou, S. Margadonna, W. Kosaka, S.-i. Ohkoshi, M. Brunelli and K. Prassides, *J. Am. Chem. Soc.*, 2006, **128**, 8358–8363.
23 D. Papanikolaou, W. Kosaka, S. Margadonna, H. Kagi, S.-i. Ohkoshi and K. Prassides, *J. Phys. Chem. C*, 2007, **111**, 8086–8091.
24 B. LeGuennic, S. Borshch and V. Robert, *Inorg. Chem.*, 2007, **46**, 11106–11111.
25 D. S. Middlemiss, D. Portinari, C. P. Grey, C. A. Morrison and C. C. Wilson, *Phys. Rev. B: Condens. Matter Mater. Phys.*, 2010, **81**, 184410.
26 D. B. Brown, D. F. Shriver and L. H. Schwartz, *Inorg. Chem.*, 1968, **7**, 77–83.
27 E. Coronado, M. C. Giménez-López, G. Levchenko, F. M. Romero, V. García-Baonza, A. Milner and M. Paz-Pasternak, *J. Am. Chem. Soc.*, 2005, **127**, 4580–4581.
28 G. Halder, K. W. Chapman, P. Chupas and A. Dos Santos, *Acta Crystallogr., Sect. A: Found. Adv.*, 2014, **70**, C154.
29 K. W. Chapman, P. J. Chupas and C. J. Kepert, *J. Am. Chem. Soc.*, 2006, **128**, 7009–7014.
30 A. Simonov, T. De Baerdemaeker, H. L. B. Boström, M. L. Ríos Gómez, H. J. Gray, D. Chernyshov, A. Bosak, H.-B. Bürgi and A. L. Goodwin, *Nature*, 2020, **578**, 256–260.
31 J.-D. Cafun, J. Lejeune, F. Baudelet, P. Dumas, J.-P. Itié and A. Bleuzen, *Angew. Chem., Int. Ed.*, 2012, **51**, 9146–9148.
32 C. E. Housecroft and A. G. Sharpe, *Inorganic Chemistry*, Pearson, Harlow, 2012.
33 H. J. Shepherd, C. Bartual-Murgui, G. Molnár, J. A. Real, M. C. Muñoz, L. Salmon and A. Bousseksou, *New J. Chem.*, 2011, **35**, 1205–1210.
34 Y. S. Ye, X. Q. Chen, Y. D. Cai, B. Fei, P. Dechambenoit, M. Rouzières, C. Mathonière, R. Clérac and X. Bao, *Angew. Chem.*, 2019, **131**, 19064–19067.
35 N. Moliner, C. Muñoz, S. Létard, X. Solans, N. Menéndez, A. Goujon, F. Varret and J. A. Real, *Inorg. Chem.*, 2000, **39**, 5390–5393.
36 G. F. Turner, F. Campbell, S. A. Moggach, S. Parsons, A. E. Goeta, M. C. Muñoz and J. A. Real, *Angew. Chem.*, 2020, **59**, 3106–3111.
37 H. L. B. Boström, I. E. Collings, A. B. Cairns, C. P. Romao and A. L. Goodwin, *Dalton Trans.*, 2019, **48**, 1647–1655.
38 F. Birch, *Phys. Rev.*, 1947, **71**, 809–824.
39 F. D. Murnaghan, *Proc. Natl. Acad. Sci. U. S. A.*, 1944, **30**, 244–247.
40 R. J. Angel, M. Alvaro and J. Gonzalez-Platas, *Z. Kristallogr.*, 2014, **229**, 405–419.
41 D. M. Pajerowski, S. E. Conklin, J. Leão, L. W. Harriger and D. Phelan, *Phys. Rev. B: Condens. Matter Mater. Phys.*, 2015, **91**, 094104.
42 G. Felix, M. Mikolasek, H. J. Shepherd, J. Long, J. Larionova, Y. Guari, J.-P. Itié, A. I. Chumakov, W. Nicolazzi, G. Molnár and A. Bousseksou, *Eur. J. Inorg. Chem.*, 2018, 443–448.
43 A. L. Goodwin, K. W. Chapman and C. J. Kepert, *J. Am. Chem. Soc.*, 2005, **127**, 17980–17981.
44 A. L. Spek, *Acta Crystallogr., Sect. D: Biol. Crystallogr.*, 2009, **65**, 148–155.
45 Y. H. Zhao, M. H. Abraham and A. M. Zissimos, *J. Org. Chem.*, 2003, **68**, 7368–7373.
46 S. A. Moggach, T. D. Bennett and A. K. Cheetham, *Angew. Chem., Int. Ed.*, 2009, **48**, 7087–7089.
47 S. C. McKellar and S. A. Moggach, *Acta Crystallogr., Sect. B: Struct. Sci., Cryst. Eng. Mater.*, 2015, **71**, 587–607.
48 S. F. A. Kettle, G. L. Aschero, E. Diana, R. Rossetti and P. L. Stanghellini, *Inorg. Chem.*, 2006, **45**, 4928–4937.
49 A. Cano, L. Reguera, M. Avila, D. Velasco-Arias and E. Reguera, *Eur. J. Inorg. Chem.*, 2020, 137–145.
50 D. Collison, C. D. Garner, C. M. McGrath, J. F. W. Mosselmans, M. D. Roper, J. M. W. Seddon, E. Sinn and N. A. Young, *J. Chem. Soc., Dalton Trans.*, 1997, 4371–4376.
51 S. Decurtins, P. Gütlich, C. P. Köhler, H. Spiering and A. Hauser, *Chem. Phys. Lett.*, 1984, **105**, 1–4.
52 D. Unruh, P. Homenya, M. Kumar, R. Sindelar, Y. Garcia and F. Renz, *Dalton Trans.*, 2016, **45**, 14008–14018.
53 G. Vankó, F. Renz, G. Molnár, T. Neisius and S. Kárpáti, *Angew. Chem., Int. Ed.*, 2007, **46**, 5306–5309.
54 C. Wäckerlin, F. Donati, A. Singha, R. Baltic, S. Decurtins, S.-X. Liu, S. Rusponi and J. Dreiser, *J. Phys. Chem. C*, 2018, **122**, 8202–8208.
55 R. D. Shannon, *Acta Crystallogr., Sect. A: Cryst. Phys., Diffr., Theor. Gen. Crystallogr.*, 1976, **32**, 751–767.
56 A. B. Cairns, J. Catafesta, P. Hermet, J. Rouquette, C. Levelut, D. Maurin, A. van der Lee, V. Dmitriev, J.-L. Bantignies, A. L. Goodwin and J. Haines, *J. Phys. Chem. C*, 2020, **124**, 6896–6906.